Journal of Materials Chemistry A

Accepted Manuscript

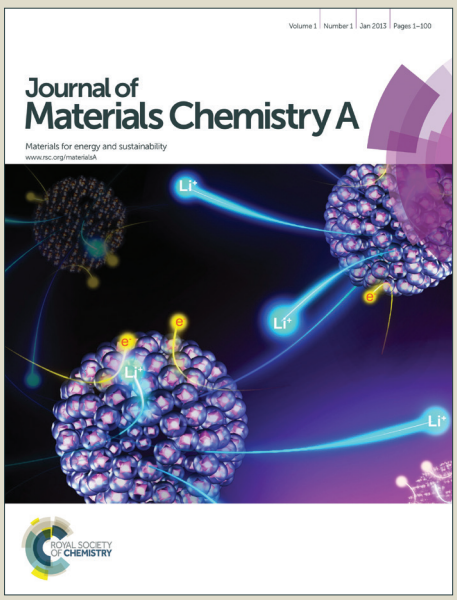

This is an *Accepted Manuscript*, which has been through the Royal Society of Chemistry peer review process and has been accepted for publication.

Accepted Manuscripts are published online shortly after acceptance, before technical editing, formatting and proof reading. Using this free service, authors can make their results available to the community, in citable form, before we publish the edited article. We will replace this *Accepted Manuscript* with the edited and formatted *Advance Article* as soon as it is available.

You can find more information about *Accepted Manuscripts* in the Information for Authors.

Please note that technical editing may introduce minor changes to the text and/or graphics, which may alter content. The journal's standard Terms & Conditions and the Ethical guidelines still apply. In no event shall the Royal Society of Chemistry be held responsible for any errors or omissions in this *Accepted Manuscript* or any consequences arising from the use of any information it contains.

ROYAL SOCIETY OF CHEMISTRY

www.rsc.org/materialsA

Journal Name

ARTICLE

Effect of 4-tert-butylpyridine on Perovskite Formation and Performance of Solution-Processed Perovskite Solar Cells

Received 00th January 20xx,
Accepted 00th January 20xx

DOI: 10.1039/x0xx00000x

www.rsc.org/

Yantao Shi,*[a] Xiangyuan Wang,[a] Hong Zhang,[a] Bo Li,[a] Huilan Lu,[a] Tingli Ma,[b] Ce Hao[a]

To obtain highly efficient perovskite solar cells (PSCs), effective controls on perovskite crystallinity, homogeneity, and surface morphology are crucial. Herein, we demonstrate the flexible and facile use of TBP to improve the crystallinity of perovskite in two-step or one-step route. For the two-step route, addition of TBP into DMF when dissolving PbI_2 for spin-coating resulted in a porous layer composed of randomly packed PbI_2 nanocrystals. This approach subsequently offered a widely enlarged contact area to facilitate interfacial reaction with CH_3NH_3I and greatly improved $CH_3NH_3PbI_3$ crystallization. Based on this strategy, the PCEs of the $CH_3NH_3PbI_3$-based PSCs were improved from 6.71% to 10.62% (i.e., 58% enhancement). For one-step route, TBP as an additive resulted in orientational and better crystallinity, by which the PCEs of $CH_3NH_3PbI_{3-x}Cl_x$-based planar PSCs increased from 11.11% to 15.01%, showing a remarkable enhancement of as high as 35%. Using TBP as one multifunctional additive, it is thought that our strategy in this work offers a new idea for fabrication of highly efficient PSCs.

1. Introduction

In the past three years, organometal halide perovskites have been considered extraordinary photovoltaic materials with desirable properties, such as moderate direct band-gap, high carrier mobility, ambipolar behaviour in charge transport, and facile solution processability.[1,2] For thin-film solar cells, organometal halide perovskites are not only good photoabsorbers, but also superior charge transport media (for both electrons and holes), which facilitate high photoelectric conversion efficiencies (PCEs) and provide more flexibility in cell architecture design.[3,4] High PCEs from 9.7% in 2012 to 20.1% in 2015 have been achieved successively by perovskite solar cells (PSCs) with either mesoporous or planar architectures.[1,5] To obtain highly efficient PSCs, effective controls on perovskite crystallinity, homogeneity, and surface morphology are crucial. High-quality perovskite can be prepared by vapor-assisted methods.[6] However, solution routes are more advantageous and competitive for large-scale production. In recent years, various efforts have been exerted to upgrade solution routes and photovoltaic performances of corresponding PSCs have been improved largely.[5,7,8]

Initially, we prepared perovskite by depositing a mixture of two precursors (i.e., PbI_2 and CH_3NH_3I) in a single step onto mesoporous TiO_2 films.[1] However, the uncontrolled precipitation process in this method usually results in large morphological variations, wide distribution in photovoltaic performance, and poor reproducibility. In 2013, disadvantages of one-step method were remedied by introducing sequential deposition method that was conducted by initially depositing mesoporous TiO_2 with PbI_2; subsequently, these materials were dipped into CH_3NH_3I solution.[9] For solution routes, at the early stage, this method largely progressed from “one-step” to “two-step”, by which high PCEs of up to 15% were achieved in 2013. Nevertheless, the two-step route is unsuitable for fabrication of all kinds of PSCs, such as planar ones. Successful use of the “two-step” route mainly depends on the mesoporous scaffolds that can offer large surface area to enable sufficient contact of PbI_2 with CH_3NH_3I for perovskite formation. However, for planar PSC fabrication, the contact between two precursors usually is very limited. Thus, the PbI_2 layer, especially the part that is distant from the contact interface, cannot be fully converted into perovskite.

Recent studies revealed that the use of specific additives and solvents is extremely effective for improving perovskite crystallization and PSC performance, especially for planar PSCs fabricated via the one-step or two-step routes. Various specific processing methods were developed based on different additives, and some mechanisms were proposed accordingly. A modified two-step method is conducted by dissolving PbI_2

[a] State Key laboratory of Fine Chemicals, School of Chemistry, Dalian University of Technology, Dalian, 116024, China.
[b] School Petroleum and Chemical Engineering, Dalian University of Technology, Panjin Campus, Panjin, 124221, P. R. China.
E-mail: shiyantao@dlut.edu.cn

† Electronic supplementary information (ESI) available: XRD patterns of the PbI_2 films with detailed peak assignments. High resolution mass spectrometry (HRMS) of the TPB-guided PbI_2 and perovskite films. See DOI: XXXX

Journal of Materials Chemistry A Accepted Manuscript

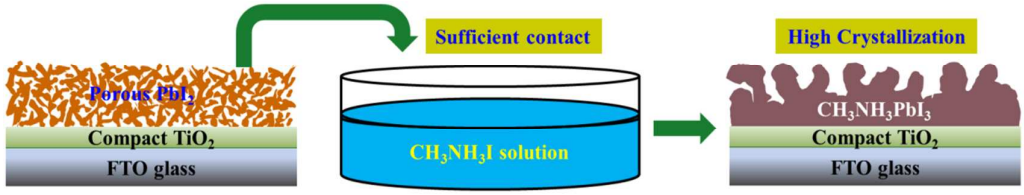

Scheme 1. Schematic diagram of the "two-step" route in which a porous and free-standing PbI_2 film is used to react with CH_3NH_3I to obtain highly crystallized $CH_3NH_3PbI_3$ perovskite.

with dimethylsulfoxide instead of N,N-dimethylmethanamide (DMF).[10] By employing this strategy, problems of incomplete conversion and uncontrolled particle sizes of perovskites were largely alleviated in the absence of mesoporous scaffold, thereby increasing film reproducibility and planar PSC. By contrast, for planar PSC fabrication by one- step routes, the additives are significant in facilitating homogeneous nucleation or crystallization kinetics modulation. Currently, highly uniform and pinhole-free perovskite films, such as $CH_3NH_3PbI_3$, $CH_3NH_3PbI_{3-x}Cl_x$, and $HC(NH_2)_2PbI_3$, have been prepared with the use of some additives, such as 1,8-diiodooctane, N-cyclohexyl-2-pyrrolidone, HI, and NH_4Cl.[11–14]

4-Tert-butylpyridine (TBP) is a commonly used additive in electrolytes of dye-sensitized solar cells[15] and in hole transport materials of PSCs.[16] In the present report, we demonstrate the flexible and facile use of TBP to improve the crystallinity of perovskite in two-step or one-step route. For the two-step route, addition of TBP into DMF when dissolving PbI_2 for spin-coating resulted in a porous layer that was constructed by randomly packing PbI_2 nanocrystals. This approach subsequently offered a widely enlarged contact area to facilitate interfacial reaction with CH_3NH_3I and greatly improved $CH_3NH_3PbI_3$ crystallization, as shown in Scheme 1. Based on this strategy, the PCEs of the $CH_3NH_3PbI_3$-based PSCs were improved from 6.71% to 10.62% (i.e., 58% enhancement). For one-step route, TBP as an additive resulted in orientational and better crystallization, by which the PCEs of $CH_3NH_3PbI_{3-x}Cl_x$-based planar PSCs increased from 11.11% to 15.01%, showing a remarkable enhancement of as high as 35%.

2. Experimental section

PSCs Fabrication. Typically, FTO glass (15 Ω sq^{-1}) was patterned by etching with Zn powder (6 −9 μm, Alfa Aesar, 97.5%) and hydrochloric acid (HCl, 4 M, Sigma-Aldrich), then followed by consequtive cleanings with 2% hellmanex solution (Sigma-Aldrich, being diluted into working concentration as received), deionized water, acetone and isopropanol, and finished through drying samples in clean air. Compact TiO_2 blocking layer (C-TiO_2) was fabricated by spin coating organic sol on the clean substrates at 3000 rpm for 30 s, followed by sintering in a furnace at 450 °C in air for 2 h. Organic sol for TiO_2 compact layer was prepared according to previous literature.[17] $CH_3NH_3PbI_3$-based PSCs were fabricated through the route of two-step sequential deposition. To prepare PbI_2 film for the normal sample, in the first step 462 mg PbI_2 (Sigma-Aldrich, 99.999%) was dissolved into 1 mL anhydrous dimethyl formamide (DMF, J&K, anhydrous, 99.8%) and then were spin-coated on C-TiO_2 /FTO substrate at 5000 rpm for 10 s, finally drying at 70 °C for 30 min in glove box. Preparation of the porous PbI_2 film for sample 2-TBP-guided-ST was conducted by adding 80 μL 4-*tert*-butylpyridine (TBP, J&K, 96%) into above PbI_2 solution (as that for sample 1-Normal-TS) and then treated with the same procedures mentioned above. After cooling to room temperature, the PbI_2 films were dipped into a solution containing 10 mg CH_3NH_3I in 1 ml 2-propanol (IPA, J&K, anhydrous, 99.5%) for 2 min, then rinsed with 2-propanol and dried at 70 °C for 30 min to form the crystallized $CH_3NH_3PbI_3$. Above two $CH_3NH_3PbI_3$ samples are named as 1-Normal-TS and 2-TBP-guided- TS, respectively, where TS refers to the "two-step" method, and 1 or 2 is the sample number. For fabrication of $CH_3NH_3PbI_{3-x}Cl_x$ normal film, one precursor solution was firstly prepared by adding 102.2 mg $PbCl_2$ (Sigma-Aldrich, 99.999%) and 174.9 mg CH_3NH_3I (with a molar ratio of 1 :3) into 500 μL anhydrous DMF and then heated at 70°C for 1 h. This sample is named as 3-Normal-OS, where "OS" represents one-step method. For sample 4-TBP-guided-OS, 40 μL TBP was added into above precursor solution additionally. $CH_3NH_3PbI_{3-x}Cl_x$ films were fabricated by spin-coating of precursor solution at 2000 rpm for 30 s. The coated films were then placed on a hot plate set at 90 °C for 1h and 100°C for 25 min. The HTM (hole transport material) prepared by dissolving 72.3 mg spiro-MeOTAD (Borun Company, China, 98%), 28.8 μl TBP, and 20 μl solution of 300 mg ml^{-1} Co(III) TFSI salt ($Co[PyPz]_3[TFSI]_3$,MaterWin Technology, >99%) in acetonitrile, and 17.5 μl solution of 520 mg ml^{-1} lithium bis(trifluoromethylsulphonyl)imide (LiTFSI, Sigma-Aldrich, 99.95%) in acetonitrile (J&K, 99.8%) into 1 ml chlorobenzene (Alfa Aesar, 99.5%) was deposited by spin coating at 3000 rpm for 30 s. Finally, the fabrication of PSCs was completed after depositing 100 nm Ag (Alfa Aesar, 99.9%) by means of thermally evaporation on top of the HTM layer. The active area of this electrode was fixed at 0.12 cm^2.

Characterizations: Microscopic morphology and crystallinity were characterized by scanning electron microscopy (SEM, FEI Quanta 450) and X-ray diffraction (XRD, D/Max-2400, Rigaku), respectively. The UV-Vis absorbance spectra of perovskite were measured with a UV-Vis spectrophotometer (HP 8453, Hewlett Packard, USA) by deducting the background of the compact TiO_2 layer. Photocurrent-voltage (*J-V*) curves were measured under AM 1.5, 100mW cm^{-2} irradiation (PEC-L15, Peccell, Yokohama, Japan) by a Keithley digital source meter (Keithley 2601, USA). Before each *J-V* measurement, the light intensity was calibrated with a standard crystalline silicon solar cell. IPCE measurements were performed using a monochromatic light from a system made of a xenon lamp, a monochromator, and appropriate filters.

Journal of Materials Chemistry A Accepted Manuscript

This journal is © The Royal Society of Chemistry 20xx

3. Results and discussion

As shown in Figures 1a and 1b, a relatively compact PbI_2 film approximately 100 nm in thickness was obtained through the normal route. After the reaction with CH_3NH_3I solution, larger and closely packed $CH_3NH_3PbI_3$ crystals were formed in sample 1-normal-TS with sizes ranging from 200 nm to 500 nm, as shown in Figures 1c and 1d. For TBP-guiding, we obtained a free-standing and porous PbI2 film composed of randomly packed nanoparticles, as illustrated in Figures 1e and 1f. The porous PbI_2 film is more advantageous compared to the compact one because a greatly enlarged surface area is available for the subsequent reaction with CH_3NH_3I solution,

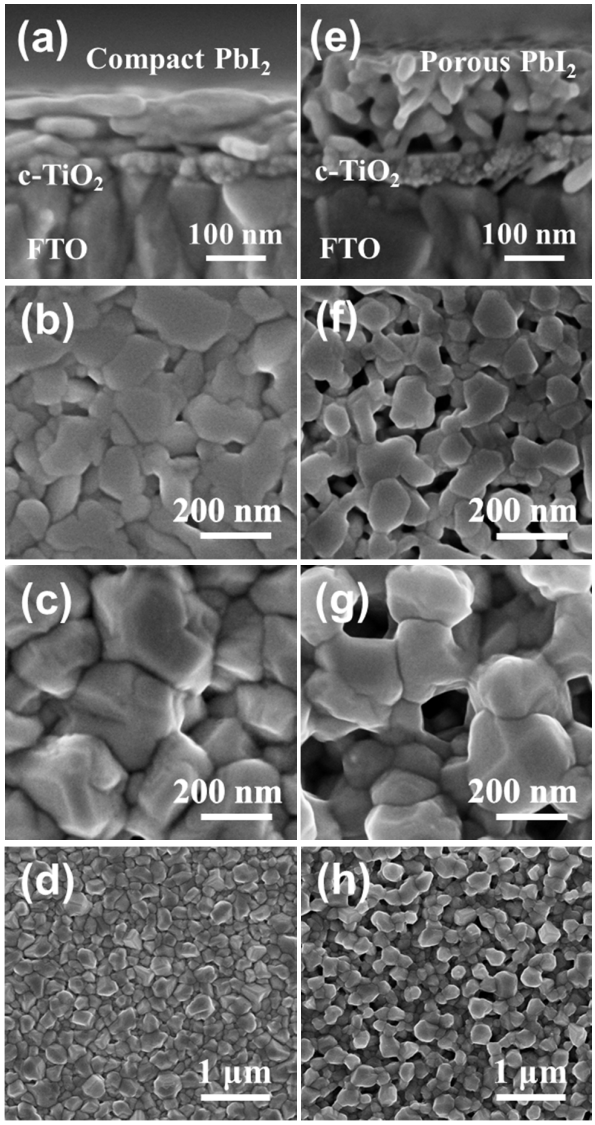

Figure 1. SEM images of PbI_2 film and $CH_3NH_3PbI_3$ films. (a) and (b): compact PbI_2 film prepared without TBP-guiding; (c) and (d): $CH_3NH_3PbI_3$ film (sample 1-Normal-TS) prepared using the compact PbI_2 film; (e) and (f): porous PbI_2 film prepared by TBP-guiding; (g) and (h): $CH_3NH_3PbI_3$ film (sample 2-TBP-guided-TS) prepared using the porous PbI_2 film.

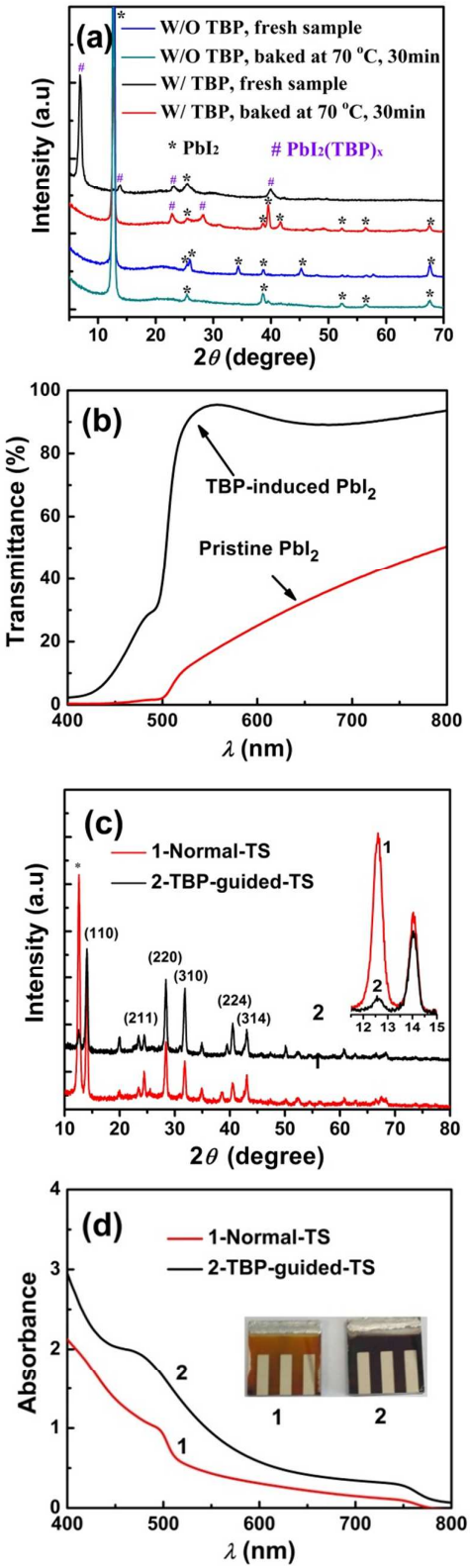

Figure 2. (a) XRD patterns of PbI_2 films; (b) transmittance spectra of PbI_2 films; (c) XRD patterns of $CH_3NH_3PbI_3$ films, the insert are the extracted part; (d) UV-Vis absorbance spectra of $CH_3NH_3PbI_3$ films, the insert are digital photos of the cells.

Journal of Materials Chemistry A Accepted Manuscript

which is necessary for full conversion of PbI_2 into $CH_3NH_3PbI_3$.

Although the mechanism by which TBP guided the formation of PbI_2 nanoparticles in the present work is unclear, we believe that the "guiding" effect of TBP is highly relevant to the coordination effect between Pb^{2+} and TBP. Compared with the oxygen atom on DMF, the nitrogen atom on TBP (pyridine nitrogen) as electron-donating unit is more inclined to coordinate with Pb^{2+}. We conjecture that such greater coordination can eventually tune PbI_2 crystallization into nanosized particles. In addition, TBP can also act as dispersing agent (similar to some surfactants) that is capable of hindering the formation of large-sized bulks or aggregates. Based on the porous PbI_2, the morphology of the resultant $CH_3NH_3PbI_3$ film for sample 2-TBP-guided-TS is very different from 1-normal-TS as this material is also porous. In addition, this material has numerous large hollow pores with diameters exceeding 100 nm. The $CH_3NH_3PbI_3$ crystals were also found to interconnect well around the pores. This condition is an important prerequisite for efficient carrier transport. To the best of our knowledge, the present study proposed a tuning method or a morphology that has never been reported.

The crystallinities of PbI_2 films prepared using the normal and TBP-guided, two-step routes were characterized by X-ray diffraction (XRD), as shown in Figure 2a. Furthermore, to probe the evolution of crystallinity of PbI_2 before and after heating, one fresh film (drying in air, without baking) and one baked at 70 °C for 30 min were measured. Detailed assignments of the diffraction peaks for each curve in Figure 2a are demonstrated in Figure S1. For the PbI_2 sample prepared without TBP guiding, all diffraction peaks in either the fresh film or the one baked at 70 °C for 30 min correspond well to PbI_2, suggesting no formation of crystallized PbI_2-DMF complex. On the other hand, the PbI_2 crystallization in the case of using only DMF as solution is highly oriented. This result is consistent with that reported previously.[10] By contrast, based on the strong and strange diffraction peaks (marked with "#") observed in the fresh film with TBP guiding, it is evident that PbI_2-TBP complex has been formed. Even after baking at 70 °C for 30 min, peaks (at 2θ = 22.8 ° and 28.1 °) that belong to PbI_2-TBP complex also exist. XRD results indicate that TBP and PbI_2 have strong interaction, under which a intermediate (one complex) can be formed in the preparation of PbI_2 film. In light transmittance measurement from 500 nm to 800 nm, the porous PbI_2 film allows the transmission of above 80% incident light, as illustrated in Figure 2b. By contrast, only a small fraction of incident light can go through the compact PbI_2 film. This characterization actually reflects the nature of these two films, namely, compact and porous. Figure 2c shows XRD patterns of the resultant $CH_3NH_3PbI_3$ films prepared according to the two different two-step routes. In 1-normal-TS sample, a substantial portion of PbI_2 was apparently not converted into $CH_3NH_3PbI_3$ because the characteristic peak intensity for PbI_2 (001) plane is still very strong. By contrast, in 2-TBP-guided TS sample, the diffraction peak for PbI_2 is relatively very weak, as clearly illustrated by the comparison in the insert of Figure 2c. This finding also suggests that our TBP-guided route is very facile and effective. For the normal two-step route, such problem may be resolved through reaction time alteration. However, extending the dipping time in CH_3NH_3I solution is not feasible because this process will result in the formation of extremely large crystals (several microns), which hinder electron transport through perovskite film and deteriorate charge recombination.[10] As shown in Figure 2d, 2-TBP-guided TS samples shows relatively high absorbance in the whole visible and some near-infrared light regions because of good crystallinity. By comparison, the PSC based on 2-TBP-guided TS is darker than the one based on 1-normal-TS, as illustrated in the inset of Figure 2d. By high resolution mass spectrometry (HRMS), we confirmed that TBP has been fully

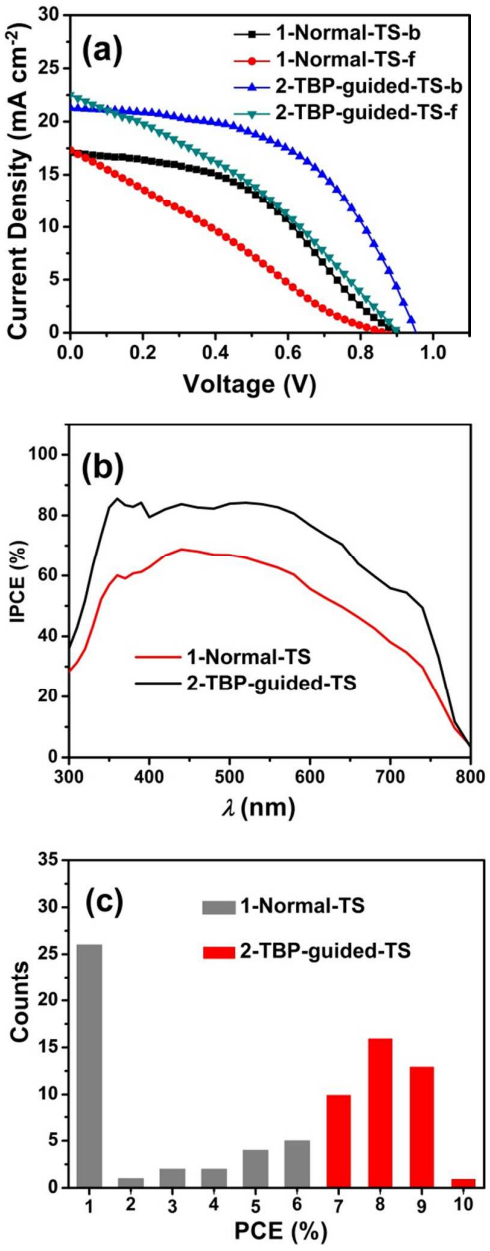

Figure 3. (a) Photocurrent-photovoltage (*J-V*) curves of the PSCs fabricated according to the two two-step routes; (b) IPCE

Journal of Materials Chemistry A Accepted Manuscript

This journal is © The Royal Society of Chemistry 20xx

curves of the PSCs; (c) Distribution diagrams of power conversion efficiencies (PCEs) from $CH_3NH_3PbI_3$-based PSCs.

Table 1. Detailed photovoltaic parameters of the PSCs fabricated by two-step route.

Sample		Scan mode	V_{OC} (V)	J_{SC} (mA cm^{-2})	FF (%)	PCE (%)
1-Normal-TS	Average	Reverse scan	0.83 ± 0.06	8.05 ± 5.68	0.37 ± 0.06	2.55 ± 2.07
	Champion	Reverse scan	0.92	17.12	0.43	6.71
		Forward scan	0.88	17.32	0.26	3.88
2-TBP-guided-TS	Average	Reverse scan	0.90 ± 0.04	19.58 ± 1.00	0.49 ± 0.04	8.66 ± 0.82
	Champion	Reverse scan	0.96	21.27	0.52	10.62
		Forward scan	0.92	22.50	0.34	7.06

removed after the formation of TBP-guided perovskite film (see Figure S2 and S3 in supporting information).

Figure 3a illustrates the J–V curves of the champion devices based on the PSCs fabricated via the two different two-step routes; the J–V curves were measured under AM 1.5 and 100 mW cm^{-2} simulated light. Detailed photovoltaic parameters including that of the champion devices and the mean values of 35 devices for each group are summarized in Table 1. For 1-normal-TS-based PSCs, the mean PCE is extremely low, which is only 2.55% (Table 1). Low short-circuit current density (J_{sc}) and fill factor (*FF*) are specifically responsible for the unsatisfactory results. Previous studies reported that in some conditions, residual PbI_2 in perovskite was advantageous to PSC performance. This outcome was caused by the finding that proper amount (usually very small) of PbI_2 is favorable in the suppression charge-recombination at the TiO_2/perovskite interface or grain boundaries of perovskite crystals. Meanwhile, in 1-normal-TS sample, the amount of residual PbI_2 was relatively large (as confirmed by XRD results mentioned above); therefore, transport and collection of photo-generated electrons would be affected seriously. Consequently, we can obtain neither large J_{sc} nor *FF* because the residual PbI_2 will directly result in the increase in series resistance (R_s) and deterioration in charge-recombination. For 1-normal-TS-based PSCs, another serious problem is the poor reproducibility. Table 1 also shows that the J_{sc} value shows an extremely large distribution, which further confirms the poor controllability when using the normal two-step route. As demonstrated in Figure 3a, the champion device for 1-normal-TS-based PSCs exhibits a PCE of only 6.71%, whereas the one based on 2-TBP-guided-TS route provide a relatively higher PCE of 10.62%, which was greatly enhanced by 58%. All photovoltaic parameters have been found to improve for 2-TBP-guided-TS-based PSCs, wherein J_{sc} and *FF* contributed most to the final PCE. Apparently, the enhancement in photovoltaic performance was derived from the improved $CH_3NH_3PbI_3$ crystallinity. In PSCs, the hysteresis phenomenon is very common, which has generally been attributed to the migration of ions within the perovskite film or to the transient ferroelectric polarization.[18] Improving the crystallinity of the perovskite films has proved effective in term of eliminating the hysteresis phenomenon.[19] Although hysteresis still exists in 2-TBP-guided-TS-based PSCs, it has been alleviated a lot when compared to the one prepared by the normal route. Obviously, the amelioration in hysteresis was achieved as a result of the improved crystallinity of perovskite by TBP-guiding. Spectra of the monochromatic incident photon-to-electron conversion efficiency (IPCE) are shown in Figure 3b. From 300 nm to nearly 800 nm, 2-TBP-guided-TS-based device was more efficient than 1-normal-TS-based device and exceeds 80% in the region from 355 nm to 560 nm. Moreover, based on this modified two-step route, the reproducibility has also improved greatly, as shown in Figure 3c. In 2013, Snaith proposed three probable future directions for PSC technology, including the "porous perovskite p-n heterojunction" architecture, which is similar to the bulk heterojunction organic solar cells.[17] Compared to planar p-i-n cell architecture, the "porous p-n heterojunction" may benefit from the enlarged interfacial contact between perovskite and charge-selective material, which is favorable to the extraction of photogenerated carriers. However, no report still has been published regarding such PSCs. Therefore, our research study may provide one important idea for fabrication of "porous perovskite p-n heterojunction" PSCs.

For one-step routes, additives are very effective in promoting homogeneous crystallization of high-quality

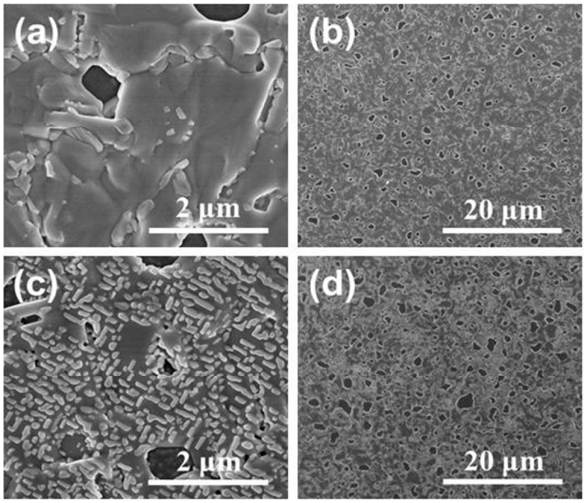

Figure 4. SEM images of $CH_3NH_3PbI_{3-x}Cl_x$ layers. (a) and (b) the one fabricated by normal one-step route (sample 3-Normal-OS); (c) and (d) the one fabricated by TBP-guided one-step route (sample 4-Normal-OS).

perovskite films for planar p-i-n junction PSCs. In the present work, the abovementioned results motivated us to use TBP in

Journal of Materials Chemistry A Accepted Manuscript

the one-step route. Regardless of the chemical components, $PbCl_2$ is used as precursor in preparing $CH_3NH_3PbI_{3-x}Cl_x$.[20–22] We also introduced TBP into the $CH_3NH_3PbI_{3-x}Cl_x$ synthesis via the one-step route. Details of the synthesis can be found in the Experimental section. The 3-normal-OS samples were prepared by the normal one-step route. This $CH_3NH_3PbI_{3-x}Cl_x$ film was condensed using numerous pinholes, as illustrated in Figures 4a and 4b. In addition, we can hardly find any isolated and distinguishable crystals as observed in $CH_3NH_3PbI_3$ samples because of the fused grain boundaries. Similar to other additives, initial TBP was expected to be able to promote homogeneous nucleation and result in high-quality $CH_3NH_3PbI_{3-x}Cl_x$ film. However, the 4-TBP-guided-OS sample we obtained using this strategy was not a pinhole-free film, as shown in Figures 4c and 4d. However, at least two different crystallization forms can be found in Figure 4c. Similar to sample 3-normal-OS, the first form exhibits smooth surface and large scale. Meanwhile, the second crystallization form is composed of large quasi-cuboid-like crystals that are formed from the first crystallization, which are approximately hundreds and tens of nanometers in length and width, respectively. We infer that the formation of these crystals is

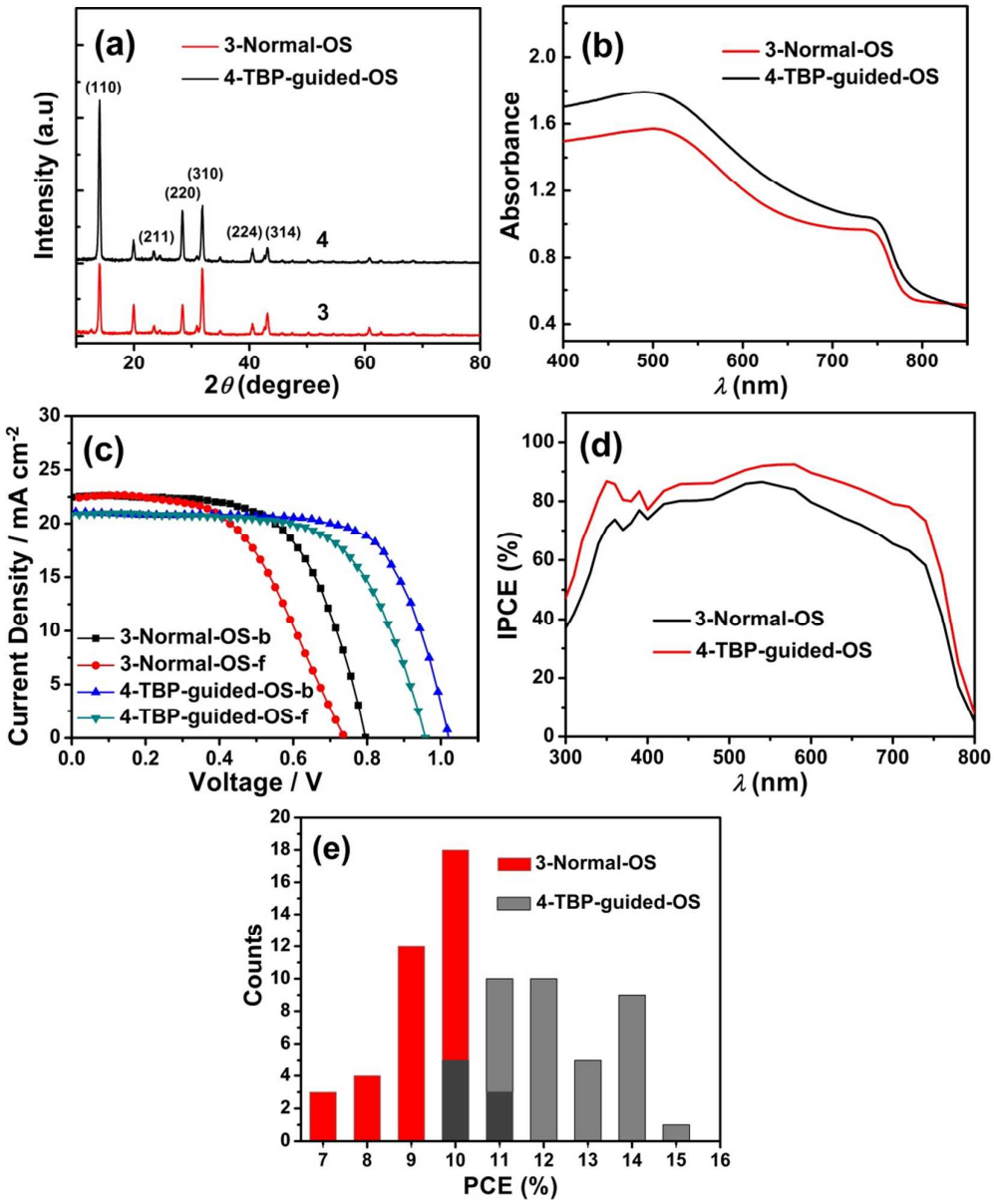

Figure 5. (a) XRD patterns of $CH_3NH_3PbI_{3-x}Cl_x$ films; (b) UV-Vis absorbance spectra of $CH_3NH_3PbI_{3-x}Cl_x$ films; (c) *J-V* curves of $CH_3NH_3PbI_{3-x}Cl_x$-based PSCs; (d) IPCE curves of $CH_3NH_3PbI_{3-x}Cl_x$-based PSCs; (e) Distribution diagrams of PCEs of $CH_3NH_3PbI_{3-x}Cl_x$-based PSCs.

Journal of Materials Chemistry A Accepted Manuscript

This journal is © The Royal Society of Chemistry 20xx

Table 2. Detailed photovoltaic parameters of the PSCs fabricated by one-step route.

Sample		Scan mode	V_{OC} (V)	J_{SC} (mA cm^{-2})	FF (%)	PCE (%)
3-Normal-OS	Average	Reverse scan	0.82 ± 0.05	19.94 ± 2.28	0.61 ± 0.06	9.86 ± 0.94
	Champion	Reverse scan	0.82	22.47	0.61	11.11
		Forward scan	0.76	22.43	0.52	8.74
4-TBP-guided-OS	Average	Reverse scan	0.90 ± 0.06	21.62 ± 1.98	0.65 ± 0.06	12.64 ± 1.40
	Champion	Reverse scan	1.04	21.09	0.69	15.01
		Forward scan	0.98	20.81	0.64	12.96

due to the preferred orientation of crystals caused by TBP. Finally, it is confirmed that TBP has been fully removed after the formation of TBP-guided $CH_3NH_3PbI_{3-x}Cl_x$ film (see Figure S4). The XRD patterns in Figure 5a indicate that, compared to sample 3-normal-OS, the crystallization of sample 4-TBP-guided-OS shows preferred orientation along (110) direction as the evident increases for diffraction intensities of (110) and (220) planes are observed when compared with (310) or (211). Usually, the difference in the crystallinity for perovskite film may lead to the change in properties. For example, the two samples show different UV-vis absorbance. Figure 5b shows that TBP-guided perovskite film prevails the normal sample in the whole range from 400 nm to 800 nm, which possibly has been caused by better crystallinity when compared to the normal sample (3-Normal-OS).

A total of 35 cells were examined for each sample. The average and highest performances are summarized in Table 2. 4-TBP-guided-OS-based PSCs exhibit much higher photovoltaic performance than the 3-normal-OS-based PSCs. 3-Normal-OS-based PSCs shows an average PCE of 9.86%, whereas all parameters including J_{sc}, V_{oc} and *FF* of 4-TBP-guided-OS-based PSCs enhance obviously, and finally resulting in a higher PCE of 12.64%. Figure 5d illustrates the champion cells for each $CH_3NH_3PbI_{3-x}Cl_x$ sample. The V_{oc} of 4-TBP-guided-OS-based cell is 1.04 V, which is evidently higher than that of 0.82 V for 3-normal-OS-based cell. Along with the notable enhancement in *FF* (0.69), a high PCE of 15.01% was obtained for a planar $CH_3NH_3PbI_{3-x}Cl_x$-based PSC. Due to the better crystallinity, the hysteresis phenomenon in 4-TBP-guided-OS-based cell is less pronounced than that observed in the 3-Normal-OS-based one. Furthermore, IPCE spectra shown in Figure 5d indicate that, in a very broad range from 300 nm to 750 nm, the two $CH_3NH_3PbI_{3-x}Cl_x$-based PSCs demonstrate high external quantum efficiency. In particular, IPCE of the 4-TBP-guided-OS-based PSC exceeds 80% from 350 nm to 700 nm. In addition to higher *PCE*, PSCs fabricated with the two $CH_3NH_3PbI_{3-x}Cl_x$ samples also show better reproducibility than the $CH_3NH_3PbI_3$-based PSCs, as shown in Figure 5e. Tuning of the crystallinity in the current study varies from that in previous studies that focused on obtaining larger crystals or pinhole-free films. Our findings suggest that using functional additives such as TBP could also result in better crystallinity. We provide a novel strategy for future studies. We believe that further enhancement of the photovoltaic performance may still be achieved by eliminating the pinholes.

Conclusions

In summary, we demonstrated a novel strategy for tuning perovskite crystallization in PSCs by a flexible and facile method involving the use of TBP in one-step and two-step routes. For two-step routes, porous PbI_2 could be constructed, which then offered an extremely enlarged contact area to facilitate interfacial reaction with CH_3NH_3I and greatly improved $CH_3NH_3PbI_3$ crystallization. Based on this strategy, the highest PCEs of the $CH_3NH_3PbI_3$-based PSCs were improved from 6.71% to 10.62% (i.e., 58% enhancement). Furthermore, TBP was also used as effectively as additive for a one-step route in fabricating $CH_3NH_3PbI_{3-x}Cl_x$-based planar PSCs. The use of TBP resulted in orientational and better crystallinity. This feature plays a positive role in increasing the photovoltage of materials. Finally, the PCE of $CH_3NH_3PbI_{3-x}Cl_x$-based PSCs exhibited a remarkable enhancement of as high as 35% (i.e., from 11.11% to 15.01%).

Acknowledgements

This work was financially supported by the National Natural Science Foundation of China (Grant No. 51402036, 51273032 and 91333104), and the International Science & Technology Cooperation Program of China (Grant No. 2013DFA51000), and the Fundamental Research Funds for the Central Universities (Grant No. DUT15YQ109).

Notes and references

(1) Kim, H.-S.; Lee, C.-R.; Im, J.-H.; Lee, K.-B.; Moehl, T.; Marchioro, A.; Moon, S.-J.; Humphry-Baker, R.; Yum, J.-H.; Moser, J. E.; Graetzel, M.; Park, N.-G. Lead Iodide Perovskite Sensitized All-Solid-State Submicron Thin Film Mesoscopic Solar Cell with Efficiency Exceeding 9%. *Sci. Rep.* **2012**, 2, 1-7.

(2) Jung, H. S.; Park, N.-G. Perovskite Solar Cells: From Materials to Devices. *Small* **2015**, 11, 10-25.

(3) Stranks, S. D.; Eperon, G. E.; Grancini, G.; Menelaou, C.; Alcocer, M. J. P.; Leijtens, T.; Herz, L. M.; Petrozza, A.; Snaith, H. J. Electron-Hole Diffusion Lengths Exceeding 1 Micrometer in an Organometal Trihalide Perovskite Absorber. *Science* **2013**, 342, 341-344.

(4) Peng, G.; Gratzel, M.; Nazeeruddin, M. K. Organohalide lead perovskites for photovoltaic applications. *Energy & Environmental Science* **2014**, 7, 2448-63.

Journal of Materials Chemistry A Accepted Manuscript

(5) Yang, W. S.; Noh, J. H.; Jeon, N. J.; Kim, Y. C.; Ryu, S.; Seo, J.; Seok, S. I. High-performance photovoltaic perovskite layers fabricated through intramolecular exchange. *Science* **2015**, 348 , 1234-1237.
(6) Liu, M.; Johnston, M. B.; Snaith, H. J. Efficient planar heterojunction perovskite solar cells by vapour deposition. *Nature* **2013**, 501 (7467), 395-398.
(7) Jeon, N. J.; Noh, J. H.; Kim, Y. C.; Yang, W. S.; Ryu, S.; Il Seol, S. Solvent engineering for high-performance inorganic-organic hybrid perovskite solar cells. *Nature Materials* **2014**, 13, 897-903.
(8) Jeon, N. J.; Lee, H. G.; Kim, Y. C.; Seo, J.; Noh, J. H.; Lee, J.; Seok, S. I. o-Methoxy Substituents in Spiro-OMeTAD for Efficient Inorganic-Organic Hybrid Perovskite Solar Cells. *J. Am. Chem. Soc.* **2014**, 136 , 7837-7840.
(9) Burschka, J.; Pellet, N.; Moon, S.-J.; Humphry-Baker, R.; Gao, P.; Nazeeruddin, M. K.; Graetzel, M. Sequential deposition as a route to high-performance perovskite-sensitized solar cells. *Nature* **2013**, 499, 316.
(10) Wu, Y.; Islam, A.; Yang, X.; Qin, C.; Liu, J.; Zhang, K.; Peng, W.; Han, L. Retarding the crystallization of PbI_2 for highly reproducible planar-structured perovskite solar cells via sequential deposition. *Energy & Environmental Science* **2014**, 7, 2934-2938.
(11) Po-Wei, L.; Chien-Yi, L.; Chu-Chen, C.; Fan, Z.; Williams, S. T.; Xu-Kai, X.; Jiangjen, L.; Jen, A. K. Y. Additive Enhanced Crystallization of Solution-Processed Perovskite for Highly Efficient Planar-Heterojunction Solar Cells. *Adv. Mater.* **2014**, 26, 3748-54.
(12) Jeon, Y.-J.; Lee, S.; Kang, R.; Kim, J.-E.; Yeo, J.-S.; Lee, S.-H.; Kim, S.-S.; Yun, J.-M.; Kim, D.-Y. Planar heterojunction perovskite solar cells with superior reproducibility. *Sci. Rep.* **2014**, 4.
(13) Heo, J. H.; Song, D. H.; Han, H. J.; Kim, S. Y.; Kim, J. H.; Kim, D.; Shin, H. W.; Ahn, T. K.; Wolf, C.; Lee, T.-W.; Im, S. H. Planar $CH_3NH_3PbI_3$ Perovskite Solar Cells with Constant 17.2% Average Power Conversion Efficiency Irrespective of the Scan Rate. *Adv. Mater*. **2015**, 27, 3424-3430.
(14) Chen, Y.; Zhao, Y.; Liang, Z. Non-Thermal Annealing Fabrication of Efficient Planar Perovskite Solar Cells with Inclusion of NH_4Cl. *Chem. Mater.* **2015**, 27, 1448-1451.
(15) Kusama, H.; Konishi, Y.; Sugihara, H.; Arakawa, H. Influence of alkylpyridine additives in electrolyte solution on the performance of dye-sensitized solar cell. *Sol. Energy Mater. Sol. Cells* **2003**, 80, 167-179.
(16) Zhang, H.; Shi, Y.; Yan, F.; Wang, L.; Wang, K.; Xing, Y.; Donga, Q.; Ma, T. A dual functional additive for the HTM layer in perovskite solar cells. *Chem. Commun*. **2014**, 50, 5020-5022.
(17) Snaith, H. J. Perovskites: The Emergence of a New Era for Low-Cost, High-Efficiency Solar Cells. *J. Phys. Chem. Lett*. **2013**, 4, 3623-3630.
(18) Chen, H. W.; Sakai, N.; Ikegami, M.; Miyasaka, T. Emergence of Hysteresis and Transient Ferroelectric Response in Organo-Lead Halide Perovskite Solar Cells. *J. Phys. Chem. Lett*. **2015**, 6, 164-169.
(19) Nie, W.; Tsai, H.; Asadpour, R.; Blancon, J. C.; Neukirch, A. J.; Gupta, G.; Crochet, J. J.; Chhowalla, M.; Tretiak, S.; Alam, M. A.; Wang, H.-L.; Mohite, A. D. High-efficiency solution-processed perovskite solar cells with millimeter-scale grains. *Science* **2015**, 347, 522-525.
(20) Lee, M. M.; Teuscher, J.; Miyasaka, T.; Murakami, T. N.; Snaith, H. J. Efficient Hybrid Solar Cells Based on Meso-Superstructured Organometal Halide Perovskites. *Science* **2012**, 338 , 643-647.
(21) Williams, S. T.; Zuo, F.; Chueh, C.-C.; Liao, C.-Y.; Liang, P.-W.; Jen, A. K. Y. Role of Chloride in the Morphological Evolution of Organo-Lead Halide Perovskite Thin Films. *Acs Nano* **2014**, 8, 10640-10654.
(22) Yu, H.; Wang, F.; Xie, F.; Li, W.; Chen, J.; Zhao, N. The Role of Chlorine in the Formation Process of "CH3NH3PbI3-xCl(x)" Perovskite. *Adv. Funct. Mater*. **2014**, 24, 7102-7108.

Journal of Materials Chemistry A Accepted Manuscript

 This journal is © The Royal Society of Chemistry 20xx

Graphical Abstract

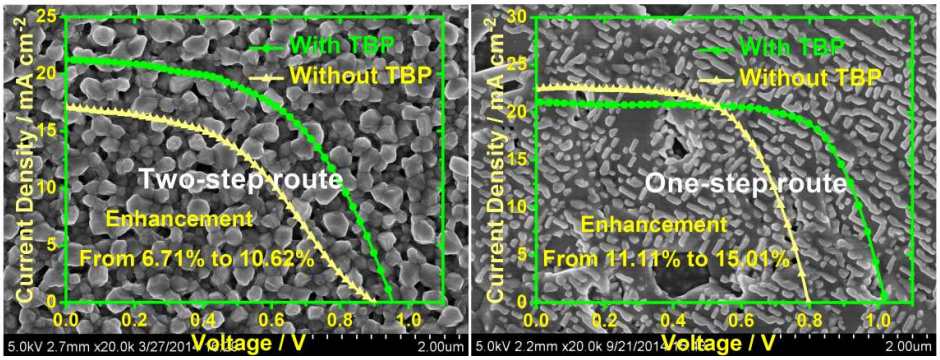

Facile use of TBP generated notable improvement on perovskite crystallinity and photovoltaic performance of perovskite solar cells.

Journal of Materials Chemistry A Accepted Manuscript